Supplementary Materials for

Genomic evidence for West Antarctic Ice Sheet collapse during the Last Interglacial Period

Sally C. Y. Lau, Nerida G. Wilson, Nicholas R. Golledge, Tim R. Naish, Phillip C. Watts, Catarina N. S. Silva, Ira R. Cooke, A. Louise Allcock, Felix C. Mark, Katrin Linse, Jan M. Strugnell

Correspondence to: cheukying.lau@jcu.edu.au

This PDF file includes:

Materials and Methods

Target capture sequencing of ddRAD loci in *P. turqueti*

Tissue samples of *Pareledone turqueti* (n = 96) collected around the Antarctic continental shelf and Antarctic islands (Fig. 1), between the depths of 102–1342 m, were sequenced with target capture probes designed from previously identified ddRADseq loci (Supplementary Text; Data S1-S2). Two outgroup species (*P. aequipapillae*; ID: 44064_1 *and P. cornuta*; ID: CT931) collected from the Ross Sea and Adélie Land were also included in the target capture dataset. For target capture sequencing, we did not include the standard DNA shearing step as these samples had already been identified as having degraded DNA. Libraries with unique index adapters were built and pooled into single capture reactions (six libraries per capture). All libraries were enriched in capture reactions using myBaits® following the manufacturer's protocol and the resulting capture reactions were sequenced on Illumina NovaSeq S4 flow cells with 150 bp paired end reads. Sixty-three *P. turqueti* samples examined in this study, as well as the two outgroup samples, were previously included in studies that analysed Cytochrome c oxidase subunit I (COI) and microsatellite data (*23*, *36*).

Target capture data processing, reads mapping and variant calling

Raw target capture reads were demultiplexed with adapters and barcodes were removed using *process_shortreads* in *Stacks* v2.3d (*37*). Reads with phred quality less than 20 (Q < 20) were also discarded, and polyG in read tails were trimmed, using *fastp* v0.20 (*38*). Potential contaminants (human and microorganisms) were identified using *Kraken* v1.0 (*39*) and sequences that were classified under the contaminant database (MiniKraken 8GB 2017) were removed. Cleaned and trimmed reads were then checked for quality using *fastQC* v0.11.7 (*40*).

Cleaned target capture reads were mapped to the consensus sequences of ddRAD loci that were used for bait design using *bwa* v0.7 (*51*) *mem* with default parameters (*41*). *Samtools* v1.7 (*42*) was used to sort alignments by coordinates, and PCR duplicates were marked and removed using *picard* v2.18.1 (*43*). Sites were called across all samples using *bcftools* v1.7 *mpileup* (*44*). Then, indels and samples with high missing data on an individual basis (> 80%) were removed, and only sites with Phred quality score higher than 30 were kept (--minQ 30). Further SNP filtering was performed differently based on the assumptions of each type of data analysis (as indicated below) using *VCFtools* v0.1.16 (*45*).

For the inference of population structure and relationship at a circumpolar scale (Principal Component Analysis [PCA], *Structure* v.2.3.4 (*46*) and *TreeMix* v.1.13 (*47*)), we included all *P. turqueti* samples (n = 96). We reduced the dataset to 5,188 biallelic unlinked SNPs, filtered based on the following steps. Sites with mean read depth of less than 16x (=average depth (48.2x) /3) and greater than 96x (=2*average depth) were removed (using --min-meanDP 16 and --max-meanDP 96). Only biallelic sites were kept (--min-alleles 2, --max-alleles 2). Sites were kept if present in at least 50% of all samples (--max-missing 0.5). Sites with a minor allele frequency of at least 5% were kept (--maf 0.05). To remove sites that likely belonged to paralogous loci and therefore artificial SNPs, only sites with a maximum observed heterozygosity of 0.5 were kept (*48*, *49*), identified via the R package *adegenet* v2.1.3 (*50*).

Lastly, only one site per locus was kept (--thin 1000; an arbitrary number larger than the longest contig, in basepair [bp] in the bait set). For the inference of admixture (*AdmixTools* v7.0.1 (*51*)), 120,857 biallelic SNPs were kept in the dataset. Instead of filtering by minor allele frequency, SNPs with a minor allele count of at least 1 were kept; and all SNPs per locus were kept.

For demographic modelling using *fastsimcoal* v2.6 (*30*), we reduced the dataset to 171,061 unlinked sites (including 115,741 biallelic SNPs) filtered based on the following steps. Sites with mean read depth of less than 17x and greater than 103x were removed (--min-meanDP 17, --max-meanDP 103). Only sites with a maximum of two alleles were kept (--min-alleles 1, --max-alleles 2). Sites were kept if present at least in 50% of all samples (--max-missing 0.5). Only sites with a maximum observed heterozygosity of 0.7 were kept (*48*, *49*), identified via the R package *adegenet*. Next, we randomly resampled a fixed number of diploid genotypes from each locality (WS: 15, AS: 4, RS: 8, EA: 5) to a dataset without missing data while maximising the number of SNPs and genotypes across localities, using a custom python script fastsimcoal/sampleKgenotypesPerPop.py. Then, within each RAD locus, SNPs in linkage disequilibrium were removed based on $r^2 > 0.95$, identified via --geno-r2 (--min-r2 0.95), following Marques et al. (2019) (*52*). We also randomly removed a number of monomorphic sites proportional to the retained number of SNPs after linkage pruning.

For inferring past population size change (*StairwayPlot* v2 (*34*, *53*)), we reduced the dataset to 106,115 biallelic SNPs. Sites with mean read depth of less than 17x and greater than 103x were removed (--min-meanDP 17, --max-meanDP 103). Only biallelic sites were kept (--min-alleles 2, --max-alleles 2). Sites were kept if present at least in 50% of all samples (--max-missing 0.5). Sites with a minor allele count of at least 1 were kept. Lastly, only sites with a maximum observed heterozygosity of 0.7 were kept (*48*, *49*), identified via the R package *adegenet*.

For *AdmixTools*, *fastsimcoal* and *StairwayPlot*, we included *P. turqueti* samples (in diploids) from WS (n = 18), AS (n = 4), RS (n = 10) and EA (n = 5; excluding Adélie Land) (Data S1). Samples from SHE (n = 13), Shag Rocks (n = 9) and South Georgia (n = 19) were also kept for *AdmixTools*. EA localities included Prydz Bay and East Casey Station; we excluded Adélie Land from EA samples as *Structure*, PCA and *TreeMix* indicated uniquely strong admixture between Adélie Land and RS in *P. turqueti*. The observed Adélie Land - RS connectivity could be linked to contemporary regional currents, thus confounding the interpretation of historical trans-West Antarctic connectivity while considering the effects of circumpolar gene flow using EA samples. Filtering thresholds were relaxed in order to retain a maximum number of informative SNPs within the scope of each model's assumptions, as the signals of true demographic events would be much stronger than a few erroneous loci (*49*).

Genetic structure of *P. turqueti*

To visualise the overall genetic structure of *P. turqueti* at a circumpolar scale, PCA was performed using *adegenet* across all samples. Individual admixture proportions were also estimated via *Structure* (*46*). *Structure* was run between $K = 1$ and 10, with ten replicates per K via *Structure_threader* (*54*). Each run was performed with 500,000 iterations and burn-in of 100,000. The meaningful K was evaluated based on the highest mean log likelihood [mean LnP(K)] and delta$K$ statistics using *Structure Harvester* (*55*).

Allele frequency correlations between seaway populations

To further explore whether there is direct admixture between seaway populations despite circumpolar gene flow driven by the Antarctic Circumpolar Current (ACC) and Antarctic Slope Current (ASC), outgroup-f_3-statistic (*29*) and *D*-statistic (in the form of BABA-ABBA) (*28*) were calculated using *AdmixTools* (*51*) via *admixr* (*56*). Both tests were constructed based on population trees and were performed between WS, AS and RS populations, with respect to locations (SHE and EA) situated in between WS, AS and RS. For both tests, samples from Shag Rocks and South Georgia were combined and considered as an outgroup population, since *Structure* analysis indicates samples from this region (Shag Rocks + South Georgia) exhibit genetic isolation. Based on mitochondrial data, *P. turqueti* from Shag Rocks and South Georgia are also considered a distinct lineage diverged from Antarctic continental shelf lineage in the mid-Pliocene (*23*).

The *D*-statistic examines whether there is excess allele sharing between two of the three ingroup populations, with respect to a common outgroup population. We considered a) whether there was a partial collapse across WAIS which would result in connectivity between WS and AS, and b) whether there was also a full collapse across WAIS which would result connectivity between WS and RS. When testing for excess allele sharing between WS and AS or RS, considering SHE or EA, we computed the *D*-statistic of the following form: *D*(seaway population, circumpolar current population, WS, outgroup), where seaway population represented AS or RS, and circumpolar current population represented those would receive potential migration via circumpolar currents (i.e. SHE or EA).

The outgroup-f_3-statistic examines the branch length between pairs of populations with respect to a common outgroup population. We computed the outgroup-f_3-statistic of the following form: f_3(Outgroup; A, B), where A and B represented pairs of population between WS, AS, RS, SHE and EA.

For *D*-statistics and outgroup-f_3-statistics, standard errors were computed with block-jackknife procedures, with blocks representing the length of RAD loci. Z-score values > 3 or < 3 were considered significantly different from 0 for both tests. Tabulated *D*-statistics and outgroup-f_3-statistics outputs are presented in table S2-S3.

SFS based inferences – mutation rate and generation time

For site frequency spectrum (SFS)-based inferences (*StairwayPlot*, *fastsimcoal*) for *P. turqueti*, a generation time of 12 years was assumed based on the species' estimated life span (*57*, *58*), as female octopods (including cold water deep-sea octopuses) are known to exhibit a single reproductive period followed by death (*57*, *59*). A mutation rate of 2.4×10^{-9} per site per generation was used based on the genome-wide mutation rate estimated for the Southern blue-ringed octopus (*Hapalochlaena maculosa*) (*60*).

Past population size changes

Past effective population size (N_e) changes within WS, AS, RS and EA populations of *P. turqueti* were reconstructed using *StairwayPlot*. *StairwayPlot* is a model-flexible method that infers past population size changes over specific points in a genealogy through 1-dimensional SFS (1d-SFS). *StairwayPlot* was chosen to further explore past population size changes instead of demographic models (e.g. *fastsimcoal*) as it is not constrained by a-priori information, which can in turn explore a larger model space than parametrised demographic models (*34*). *StairwayPlot* is also known to reconstruct recent population size changes with high accuracy comparable to whole-genome Sequentially Markovian Coalescent (SMC)-based methods (*61*). For *StairwayPlot*, we first polarised SNPs using outgroup species (*P. aequipapillae* and *P. cornuta*). Then, unfolded 1d-SFS per population was generated via easySFS.py (https://github.com/isaacovercast/easySFS#easysfs). For *StairwayPlot*, we did not project the spectra downward as the number of segregating sites are already maximised at existing sample size per population (based on easySFS). Total sequence length was defined as the length of genome explored after SNP filtering (= number of loci x length of locus). The percentage of sites used for training was 67% and the number of random break points for each run were (nseq-2)/4, (nseq-2)/2, (nseq-2)*3/4, nseq-2 based on default values. Each run was performed with a random starting seed.

Demographic modelling

We used demographic modelling to explicitly evaluate whether there were ancient migrations linking to no, partial or complete collapse of the WAIS preceding modern-day gene flow in *P. turqueti*. Demographic modelling was performed using the coalescent simulations-based framework in *fastsimcoal*. For demographic modelling, we only considered WS, AS, RS and EA in our models (4-population model), as the model evaluation is based on composite likelihoods which requires a single multidimensional SFS (i.e. four dimensional (4d)-SFS in this study). In a multidimensional SFS with > 4 populations, the number of zero entries will increase which makes it challenging for *fastsimcoal* to fit the observed data (*62*). EA samples are chosen to be included in the models instead of SHE as samples from across EA are considered of particular importance in representing clear signatures of circumpolar gene flow (*16*), because they are geographically separated from the WAIS but are also directly influenced by both the ACC and ASC.

Because there are an unlimited number of demographic models to be explored, especially when a high number of populations are incorporated (i.e. four in this study), we used a hypothesis driven, hierarchical approach to reconstruct simple, contrasting demographic models involving no, partial or complete historical collapse of WAIS using *fastsimcoal* (fig. S3). We explored simpler models and subsequently added more complex parameters to improve the fit to the observed data, as recommended by Marchi et al. (2021) (*63*), with a hierarchical framework constructed following Marques et al. (2019) (*52*). First, we compared six different models comprising different WAIS collapse scenarios (no, partial or complete collapse), while modelling contemporary gene flow driven by the ACC (clockwise) (step 1). These six models had the following conditions: 1) continuous circumpolar gene flow since population divergence (no collapse scenario), 2) strict isolation followed by clockwise circumpolar gene flow (no collapse scenario), 3) gene flow between WS-AS followed by clockwise circumpolar gene flow (partial collapse scenario), 4) gene flow between AS-RS followed by clockwise circumpolar

gene flow (partial collapse scenario), 5) gene flow between WS-RS followed by clockwise circumpolar gene flow (full collapse scenario), and 6) gene flow between WS-AS-RS followed by clockwise circumpolar gene flow (full collapse scenario). To infer more ecologically realistic scenarios, we considered complex models (step 2) that included contemporary gene flow following both the directionalities of the ACC (clockwise) and ASC (counter-clockwise). At step 2, we also considered two additional models with the following conditions: (7) gene flow between WS-AS and WS-RS followed by clockwise and counter-clockwise circumpolar gene flow, and (8) gene flow between AS-RS and WS-RS followed by clockwise and counter-clockwise circumpolar gene flow (fig. S3-S4).

Model run and selection

For *fastsimcoal* analyses, we first polarised SNPs using outgroup species (*P. aequipapillae* and *P. cornuta*). Then, we converted the datasets into unfolded multidimensional SFS for model evaluation using the python script fastsimcoal/vcf2sfs.py (https://github.com/marqueda/SFS-scripts/blob/master/vcf2sfs.py). For each model, we performed 100 independent runs of random starting parameter combinations, with each run pooling SFS entries with fewer than 10 SNPs in order to avoid overfitting (-C 10), consisting of 40 ECM optimisation cycles and using 500,000 coalescent simulations. We then re-estimated the likelihoods of each model, based on the maximum-likelihood estimates obtained from the best run (*_maxL.par), also using 100 independent runs and 500,000 coalescent simulations. The re-calculated likelihoods should closely approximate the true likelihoods as they are maximised under each model scenario, and the distribution of the re-calculated likelihoods should reflect the inherent stochasticity of coalescent simulations (*30*). We also introduced upper bound for the parameter T1 (divergence time estimate) as the model runs were detecting ancestral signals beyond the species evolutionary history, thus likely to confound estimation of recent parameter estimates (*64*). Introducing an upper bound of divergence estimates would also reduce the parameter space within the time period of interest (i.e. history since speciation) in complex models (*52*, *65*). The upper bound of T1 was constrained by the known conservative (median) estimate of species divergence time, which was 4 million years ago for *P. turqueti* (*23*). This divergence estimate was chosen as it was calculated using different markers than RAD loci; these divergence times were estimated using mitochondrial data of *P. turqueti* (*23*).

Model fits were evaluated based on the lowest deltaLikelihood, Akaike's information criterion (AIC) and AIC weights. We also visualised the distributions of re-estimated AIC values in order to assess the variance between model fitting runs. For the final best model, we visually inspected the fit of the observed versus expected SFS, as well as the residuals in model fitting, to evaluate whether the final selected model is approximated to the observed data (Supplementary Text).

The 95% confidence intervals (CI) of parameters of the best model were calculated using 100 replicates of non-parametric block-bootstrapped joint pairwise 2d-SFSs. The 100 bootstrapped replicates were generated via vcf2sfs.py. The length of each block was defined as the length of RAD locus. Within each replicate, the parameters under the best model scenario were estimated with 100 independent runs with 500,000 coalescent simulations, pooling SFS entries with fewer than 10 SNPs (-C 10), and 40 ECM optimisation cycles. The parameter estimates of the best run

from each bootstrapped replicate were used to compute the confidence interval, which was calculated via empirical percentiles.

Supplementary Text

Discovery of ddRADseq loci for target capture sequencing

Draft reference genome sequencing and assembly

A draft reference genome of *P. turqueti* was sequenced from two individuals collected from Elephant Island (ID: PT186) and the South Orkney Islands (ID: PT244) (Data S2). Total genomic DNA of both of these samples (gDNA) was extracted using a DNeasy Blood and Tissue Kit (Qiagen), following the manufacturer's protocol. Sample PT186 was sequenced on PacBio Sequel system (20 K insert library) with three cells which generated a total read volume of 28 Gigabase pairs (Gbp). Sample PT244 was sequenced using both 200 base pair (bp) and 500 bp insert libraries on an Illumina HiSeq X ten in 150 bp paired-end mode. One flow cell was used for the 200 bp library and two flow cells for the 500 bp. Genome size was estimated at between 3.7 Gb and 8.1 Gb based on the Illumina reads using Genomescope 2.0 (*66*). Genome assembly was performed with Redbean v2.4 (*67*) using the long-reads from PT186 and then error corrected using reads from PT244 with Pilon (*68*). The final assembly had a total length of 517 Mb from 38,290 contigs with the largest contig of 146 Kb and N50 of 16.9 Kb. It is available for download from https://www.marine-omics.net/resources/ (Direct download link from host: https://cloudstor.aarnet.edu.au/plus/s/opg7MQ0tVHtCmMN/download). We found that the mapping rate of Illumina raw reads from sample PT244 to the polished assembly was high (~92%) indicating that despite the small size of this assembly it captured the vast majority of unique genomic sequence. Nevertheless, the small assembly size compared with estimated genome size suggests that the assembly is highly incomplete, probably due to the collapse of many repetitive regions. We therefore used it purely for the purpose of identifying ddRAD and target capture loci likely to fall within repeat regions.

ddRAD library preparation, sequencing and SNP calling

As part of a wider effort to perform ddRAD sequencing across different Southern Ocean octopus species, 440 Southern Ocean octopus specimens (*Adelieledone polymorpha, A. adelieana*, *Adelieledone* sp., *Pareledone turqueti*, *P. aequipapillae*, *P. prydzensis*, *P. cornuta*, *P. subtilis*, *Pareledone* sp., *Megaleledone setebos* and *Graneledone* sp.) (Data S2) were selected for ddRADseq library preparation and sequencing. ddRADseq libraries were prepared at the Beijing Genomics Institute (BGI) Tech Solutions Co. Limited (Hong Kong) following Peterson et al. (*25*). Briefly, genomic DNA of each sample was digested with MseI and EcoRI restriction enzymes, ligated with barcoded adapters, pooled digested ligated fragments were size selected using Blue Pippin and divided into libraries. Twenty-two technical replicates were also included across libraries (see Data S2). All libraries were amplified via PCR using indexed primers and sequenced on a HiSeq X ten (at BGI).

Raw ddRAD reads were demultiplexed with barcodes and adapters removed by BGI using their in-house pipeline. Reads with phred quality less than 20 (Q < 20) were also discarded using fastp v0.20 (*38*). Potential contaminants (human and microorganisms) were identified using Kraken v1.0 (*39*), and reads that matched those of the contaminant database were removed. Cleaned and trimmed reads were checked for quality using fastQC v0.11.7 (*40*), and mapped to the draft genome of *P. turqueti* using bowtie2 v2.3.4.1 (*69*) (--very-sensitive-local). Local alignment (--very-sensitive-local) was used, following Souza et al. (*70*), since the ddRADseq dataset contains a wide variety of Southern Ocean octopod taxa that may contain structural rearrangements or variants at either ends of reads that are different from the reference (*P. turqueti*). Samtools v1.7 (*42*) was used to sort the alignments (BAM files) by coordinates. ddRAD loci were built from aligned and sorted reads, and SNPs were called, using the Stacks v2.3d gstacks module with default settings (*37*, *71*).

ddRAD loci discovery for target capture sequencing of P. turqueti

Initial assessment of raw genotype calls from Stacks indicated 155 out of 440 Southern Ocean octopus samples exhibited a high amount of missing data (> 80%), with 92 out of these 155 samples identified as *P. turqueti*. Samples with high levels of missing data were likely degraded due to long term storage. Then, a target capture bait set was designed with the intention of capturing a high proportion of the same loci in the degraded samples that were included in the ddRADseq (non-degraded) dataset. Loci discovery for this purpose was performed using a total of 285 samples comprising those with missing data less than 80% and included samples from the following species: *A. adelieana*, *A. polymorpha*, *Adelieledone* sp., *P. turqueti*, *P. aequipapillae*, *Pareledone* sp., *M. setebos*, *Graneledone* sp. (Data S2). The Stacks population module was then performed to retain sites that were present in 50% of the remaining samples (-R 0.5) with at least a minor allele frequency of 0.01 (- min-maf 0.01), which resulted in 31,142 loci retained. Discriminant analysis of principal components (DAPC) was performed via the R package adegenet v2.1.3 (*50*) to visualise potential batch effects between libraries (no batch effect was found). When the technical replicates were paired together, the replicate with the highest amount of missing data was removed.

The consensus fasta sequences of the 31,142 loci were then aligned back to the reference *P. turqueti* genome using bowtie2 with end-to-end alignment (--sensitive). Of the 31,142 loci, 8,942 loci were aligned back to the genome exactly once, while 20,123 aligned multiple times. Only the 8,942 uniquely aligning loci were retained for target capture bait design, to avoid paralogous genes which can compromise phylogenetic inference (*72*).

Bait design for the target capture sequencing of ddRAD loci in degraded P. turqueti *samples*

The consensus sequences of the filtered ddRAD loci (n = 8,942) were used for custom biotinylated RNA bait manufacturing at Arbor Bioscience (Ann Arbor, MI, USA). Input sequences were soft-masked (0.5%) for simple repeats and low-complexity regions using Repeat Masker (*73*), and candidate bait sequences were designed based on bait length (70 nucleotides per bait) and 3 X tiling per locus. Candidate baits were removed if, 1) they were greater than 25% soft-masked for simple repeats, 2) had hits to regions of the *P. turqueti* genome (this study) and the common octopus *Octopus vulgaris* genome (GenBank assembly accession:

GCA_003957725.1) (*74*) that were greater than 25% soft-masked, or 3) failed Arbor Bioscience in-house moderate Basic Local Alignment Search Tool (BLAST) parameters, which take into account the BLAST hit for a bait and predicted melting temperatures. The final myBaits© (Arbor Bioscience) panel contained 86,422 baits that targeted 8,877 ddRAD loci with at least one bait.

Extended results of demographic modelling

Demographic modelling of P. turqueti

We used a hierarchical approach to build a demographic model of Weddell Sea (WS), Amundsen Sea (AS), Ross Sea (RS) and East Antarctica (EA) populations in *P. turqueti*. We started from simple models (step 1; models only including contemporary gene flow flowing in the direction of the Antarctic Circumpolar Current [ACC]) and then increased model complexity (step 2; models including contemporary gene flow flowing in the direction of the ACC and the Antarctic Slope Current [ASC]) (fig. S3-S4). At step 1, a limited differentiation between maximised Akaike information criterion (AIC) values (median between 807539 and 807574) was observed across similar competing scenarios (psc_fulcol1, psc_nocol and psc_parcol) (table S4, fig. S5-S6). Therefore, we further evaluated step 2 models to increase complexity and to model more ecologically realistic scenarios. After incorporating competing scenarios of historical WAIS configurations and contemporary gene flow driven by the ACC and ASC, the "psccc_full_col1" model was identified as the best model (table S5, fig. S7-S8).

Overall, we obtained a very good fit of the expected and the observed site-frequency-spectrum (SFS) for *P. turqueti* (fig. S9). Among the entries of the one-dimensional (1D)-SFSs (fig. S10), there is a good fit of the expected SFS for the entries with more SNPs, with the fit of the expected SFS gradually getting poorer for entries with fewer SNPs. The poorest fits of the expected SFS were observed for the entries with a high number of derived alleles in some populations (fig. S9). This is expected as the modelled demographic scenarios aim to test simple contrasting hypothesised scenarios of whether there was no, partial or complete historical Western Antarctic Ice Sheet (WAIS) collapse, as well as accounting for the parameters of circumpolar gene flow, across four populations (WS, AS, RS and EA). We did not model for detailed demographic changes for each population in order to avoid over-parameterising the models. The unmodelled high number of derived alleles in some populations likely represent unmodelled population-level changes throughout the Quaternary glacial-interglacial cycles.

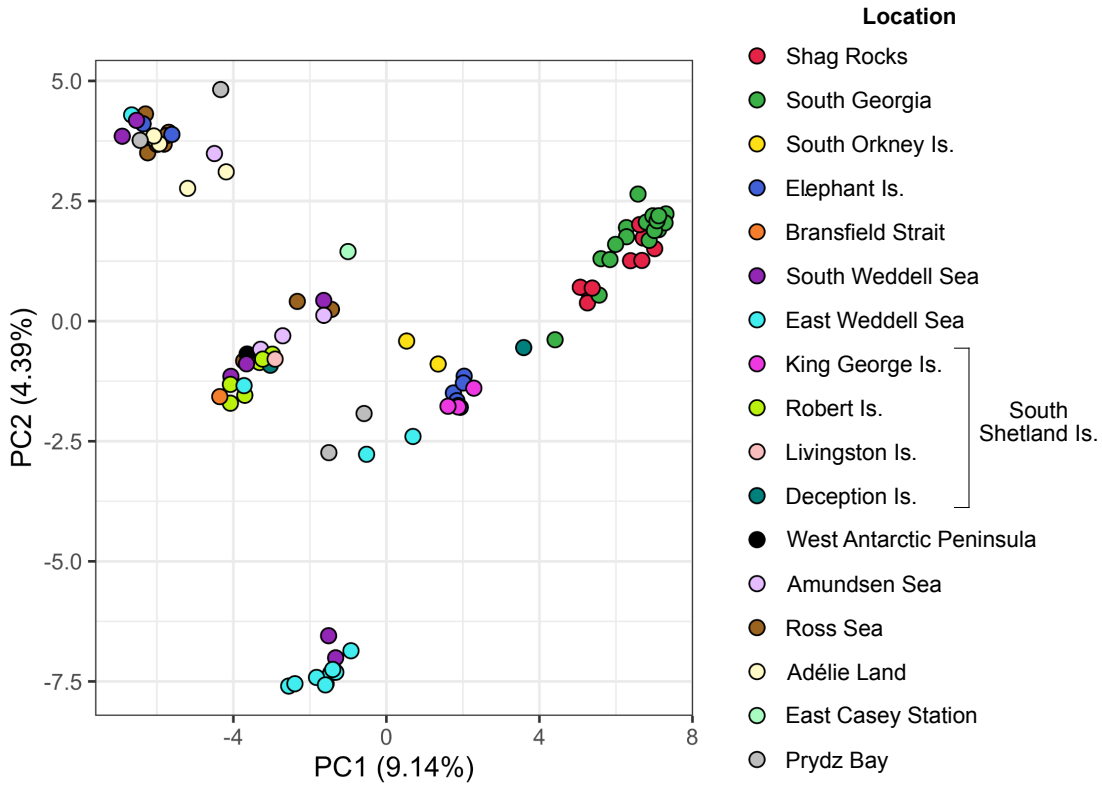

Fig. S1.

Principal component analysis (PCA) of *Pareledone turqueti*. Samples are separated by geographical locations showing the genetic variation on the first two PC axes.

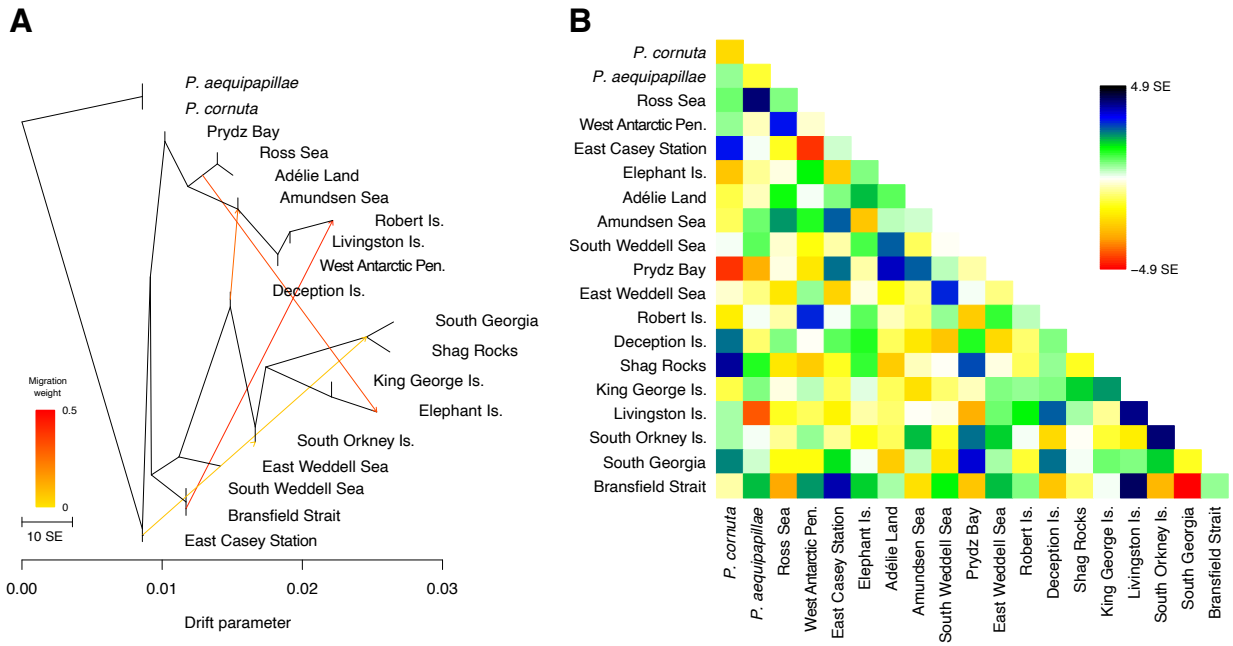

Fig. S2.

***TreeMix* maximum likelihood (ML) tree of *Pareledone turqueti* rooted with outgroups.** Horizontal branch lengths are proportional to the amount of genetic drift that has occurred on each branch. Migration edge is coloured based on migration weight, which corresponds to the % ancestry in the sink population originated from the source population. Only the edges found to be significant by jackknife significance tests were presented. (**A**) ML tree of *P. turqueti*. Terminal nodes are subdivided based on distinct geographical locations. (**B**) Residual matrix visualising the fit of the *TreeMix* modelled allele frequencies to the observed allele frequencies. Residuals are shown as the standard error (SE) of the covariance deviation. Positive residuals (> 0) represent that the *TreeMix* model underestimated the observed covariance, and that the paired populations are more closely related than modelled. Negative residuals (< 0) represent that the *TreeMix* model overestimated the observed covariance, and that the paired populations are more distant than modelled. However, negative residuals are also products of positive residuals being present in the matrix. Here the range of the residuals are small (up to ± 4.9 SE) and most are close to zero between paired localities, suggesting that the concluded *TreeMix* models were overall a good fit to the observed data.

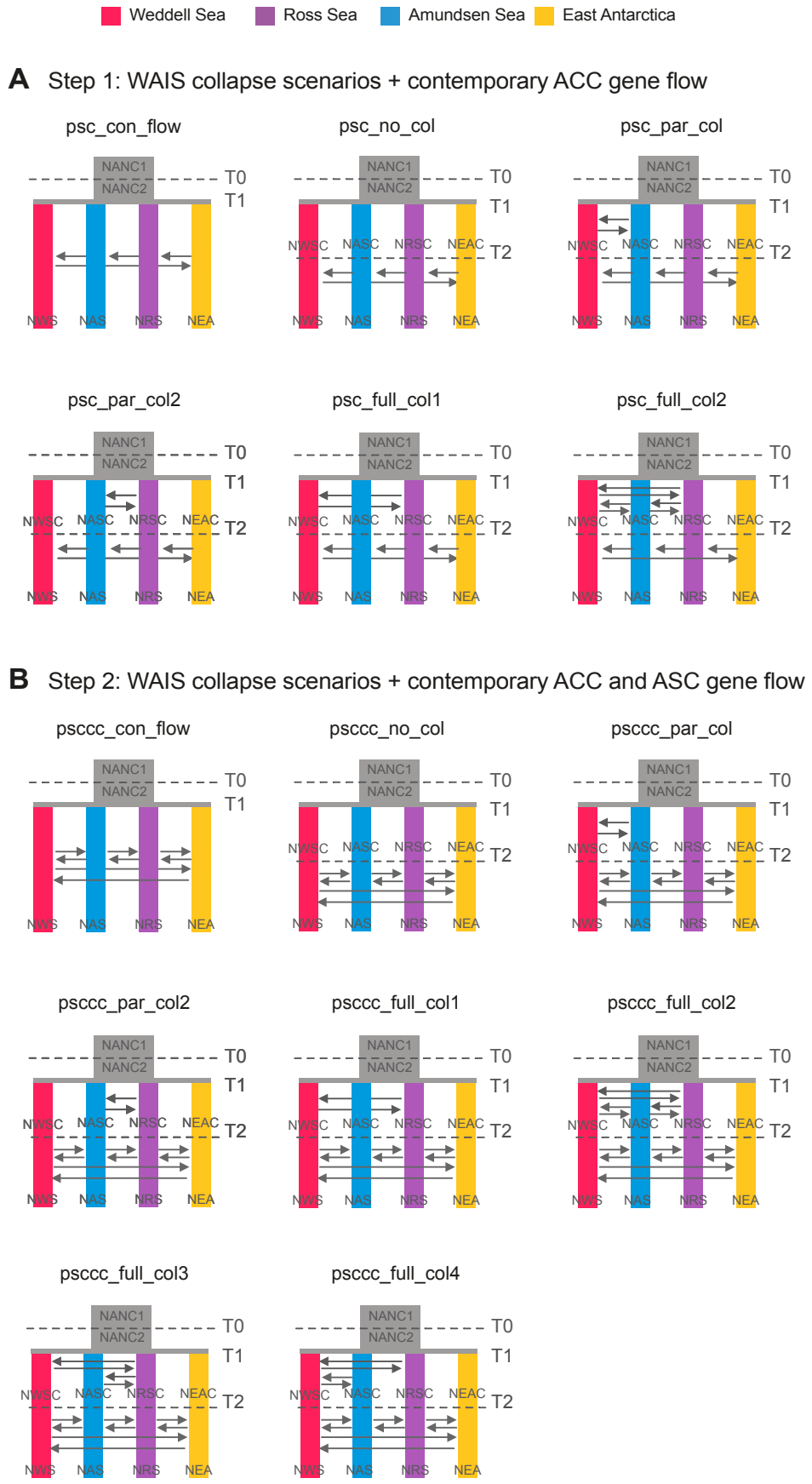
Weddell Sea
Ross Sea
Amundsen Sea
East Antarctica
A Step 1: WAIS collapse scenarios + contemporary ACC gene flow
psc_con_flow
psc_no_col
psc_par_col
psc_par_col2
psc_full_col1
psc_full_col2
B Step 2: WAIS collapse scenarios + contemporary ACC and ASC gene flow
pscccc_con_flow
pscccc_no_col
pscccc_par_col
pscccc_par_col2
pscccc_full_col1
pscccc_full_col2
pscccc_full_col3
pscccc_full_col4
NANC1
NANC2
NWSC
NASC
NRSC
NEAC
NWS
NAS
NRS
NEA
T0
T1
T2

Fig. S3.

Hierarchical demographic modelling approach to deduce signatures of historical trans-West Antarctic seaways connectivity in *Pareledone turqueti*. Simple, contrasting scenarios of past West Antarctic Ice Sheet (WAIS) configurations were compared. (**A**) For the models at step 1, it was hypothesised that since population divergence WS, AS, RS may have experienced any, partial, or complete connectivity, followed by modern circumpolar gene flow linking WS, AS, RS and EA. The possibilities of population size change over each time interval were also considered. For circumpolar gene flow, simpler models which only consisted of the directionality of the Antarctic Circumpolar Current (ACC; clockwise flowing) were performed. (**B**) To increase model complexity, step 2 models were further performed, which considered more complex models that included both directionalities of the ACC and Antarctic Slope Current (ASC; counter-clockwise flowing). Each model is labelled by the text above it. Text within each model denotes the parameter labels associated with the population size change at a particular interval (Nxxx), as well as the timing of modelled events (Tx). Dashed lines represent a distinct time interval. Arrows represent migration between populations.

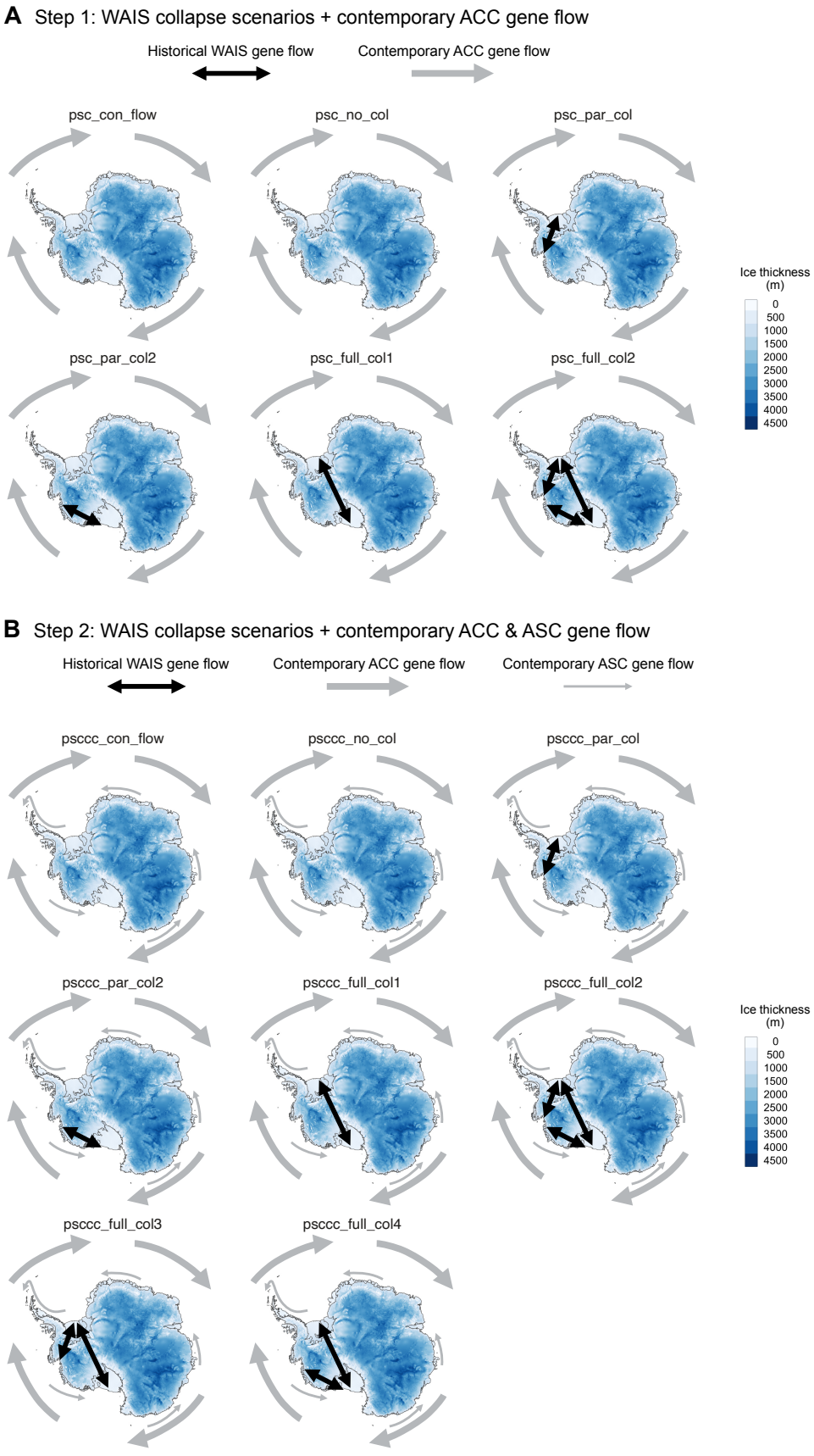
A Step 1: WAIS collapse scenarios + contemporary ACC gene flow
Historical WAIS gene flow
Contemporary ACC gene flow
psc_con_flow
psc_no_col
psc_par_col
psc_par_col2
psc_full_col1
psc_full_col2
Ice thickness (m)
0
500
1000
1500
2000
2500
3000
3500
4000
4500
B Step 2: WAIS collapse scenarios + contemporary ACC & ASC gene flow
Historical WAIS gene flow
Contemporary ACC gene flow
Contemporary ASC gene flow
psccc_con_flow
psccc_no_col
psccc_par_col
psccc_par_col2
psccc_full_col1
psccc_full_col2
psccc_full_col3
psccc_full_col4
Ice thickness (m)
0
500
1000
1500
2000
2500
3000
3500
4000
4500

413

Fig. S4.
Illustrations of the contrasting demographic models to deduce signatures of historical trans-West Antarctic seaways connectivity in *Pareledone turqueti*. (**A**) At step 1 of the hierarchical demographic modelling approach, contrasting scenarios of past Western Antarctic Ice Sheet (WAIS) configurations were compared. It was hypothesised that since population divergence, the WS, AS and RS may have experienced any, partial, or complete connectivity (black arrows), followed by contemporary circumpolar gene flow driven by the Antarctic Circumpolar Current (ACC, clockwise flowing; grey thick arrows) linking between the WS, AS, RS and EA. (**B**) At step 2, more complex models were further considered; they included both directionalities of the circumpolar gene flow, driven by the ACC (grey thick arrows) and Antarctic Slope Current (ASC, counter-clockwise flowing; grey thin arrows). Each model is labelled by the text above it. Maps illustrate ice thickness of the modern Antarctic Ice Sheet and are extracted from Bedmap2 (*32*).

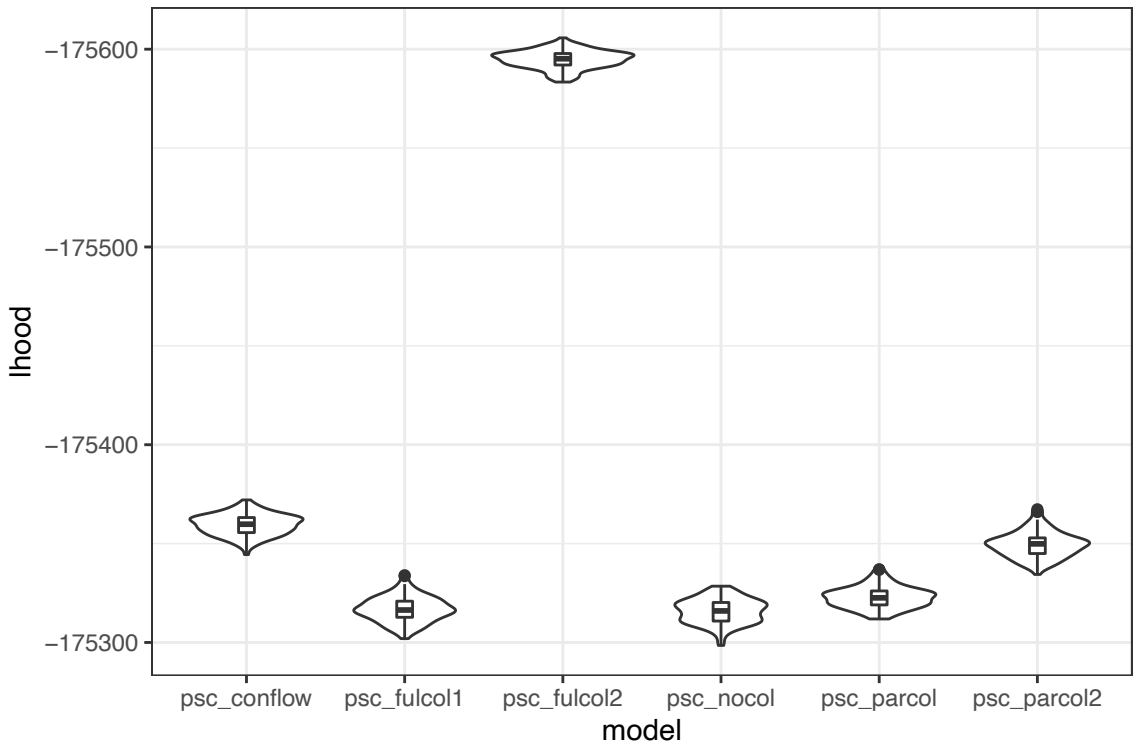

Fig. S5.
Comparisons of demographic models at step 1 in *Pareledone turqueti* (see fig. S3 for visualisations of the models). The distributions of loglikelihood (lhood) from 100 independent expected SFS (violin plot), with each approximated using 500,000 coalescent simulations under the parameters that maximised the likelihood for each model. Each box represents the interquartile range (25^{th} and 75^{th} percentile), each line represents the median, each dot represents outlier values > 1.5x and < 3x the interquartile range.

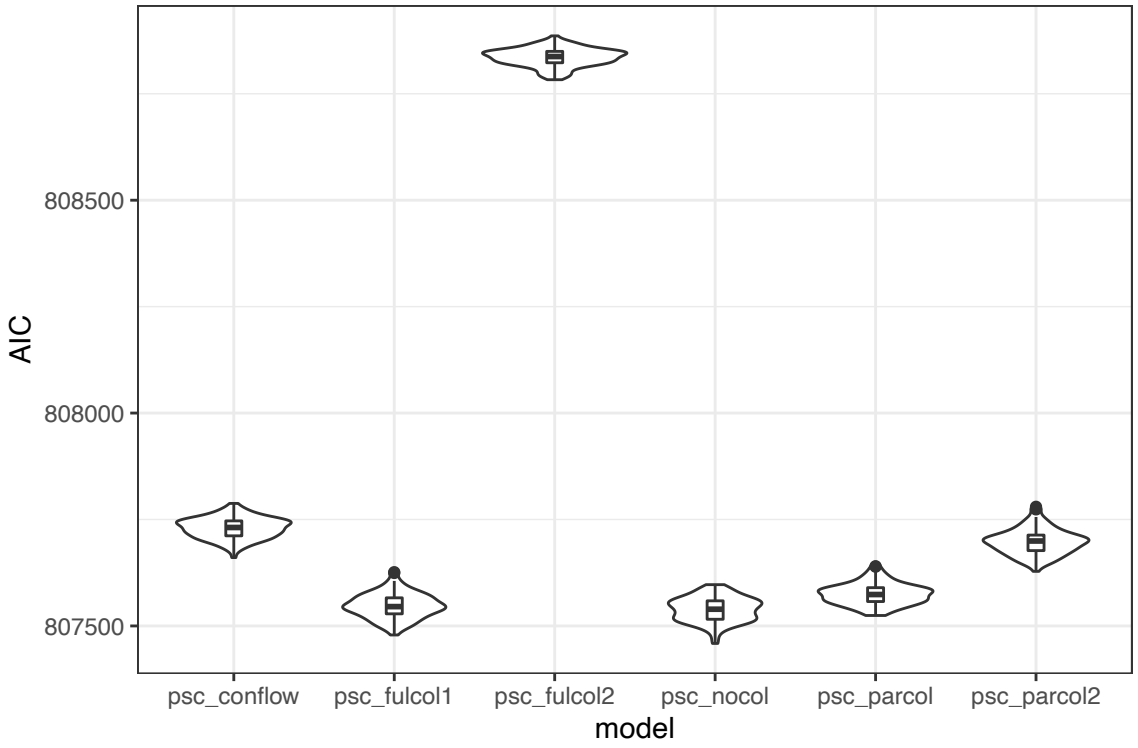

Fig. S6.

Comparisons of demographic models at step 1 in *Pareledone turqueti* (see fig. S3 for visualisations of the models). The distributions of AIC from 100 independent expected SFS (violin plot), with each approximated using 500,000 coalescent simulations under the parameters that maximised the likelihood for each model. Each box represents the interquartile range (25th and 75th percentile), each line represents the median, each dot represents outlier values > 1.5x and < 3x the interquartile range.

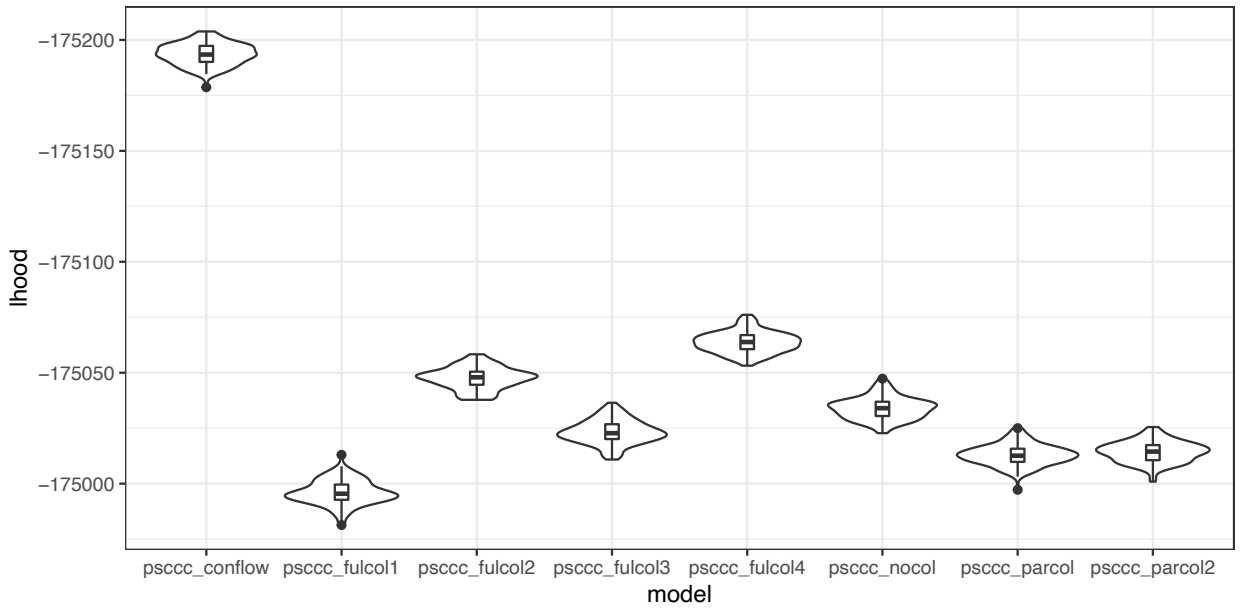

Fig. S7.

Comparisons of demographic models at step 2 in *Pareledone turqueti* (see fig. S3 for visualisations of the models). The distributions of loglikelihood (lhood) from 100 independent expected SFS (violin plot), with each approximated using 500,000 coalescent simulations under the parameters that maximised the likelihood for each model. Each box represents the interquartile range (25th and 75th percentile), each line represents the median, each dot represents outlier values > 1.5x and < 3x the interquartile range.

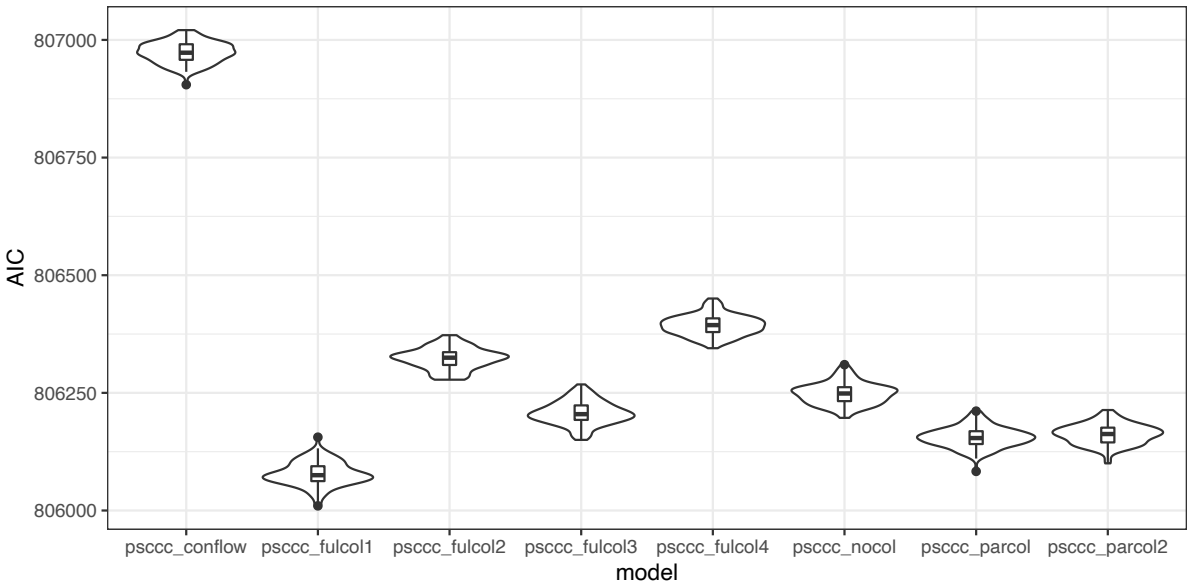

Fig. S8.

Comparisons of demographic models at step 2 in *Pareledone turqueti* (see fig. S3 for visualisations of the models). The distributions of AIC from 100 independent expected SFS (violin plot), with each approximated using 500,000 coalescent simulations under the parameters that maximised the likelihood for each model. Each box represents the interquartile range (25^{th} and 75^{th} percentile), each line represents the median, each dot represents outlier values > 1.5x and < 3x the interquartile range.

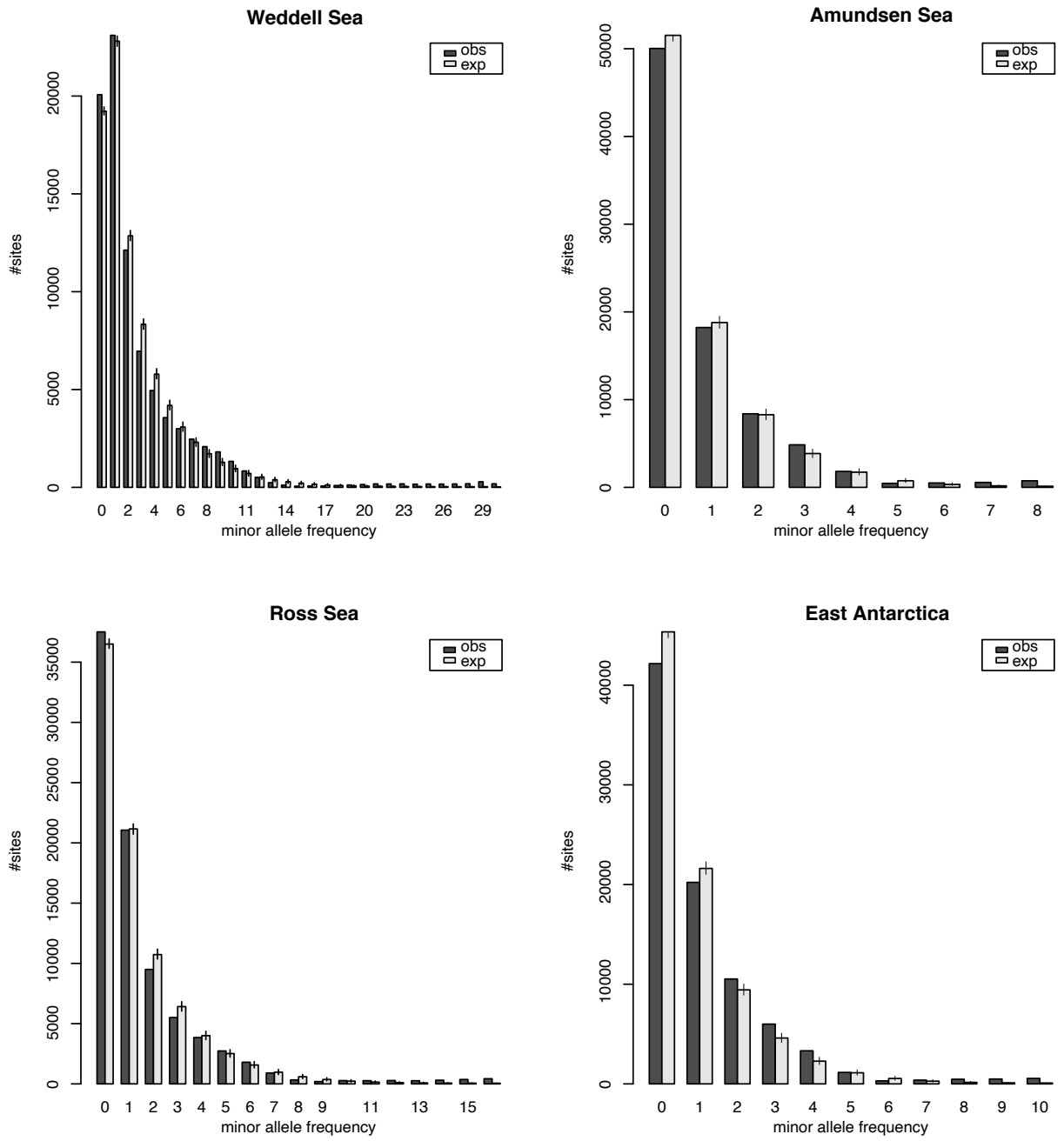

Fig. S9.

Fit of the expected and observed one-dimensional (1D)-SFS under the best model evaluated ('psccc_ful_col1') for *Pareledone turqueti*. Marginal 1D-SFS of the observed data (black bars) is compared to the averaged expected SFS (light grey bars) obtained from 100 SFS approximated with 500,000 coalescent simulations. Error bars = range of the values obtained across 100 simulated expected SFS under the parameters that maximised the likelihoods.

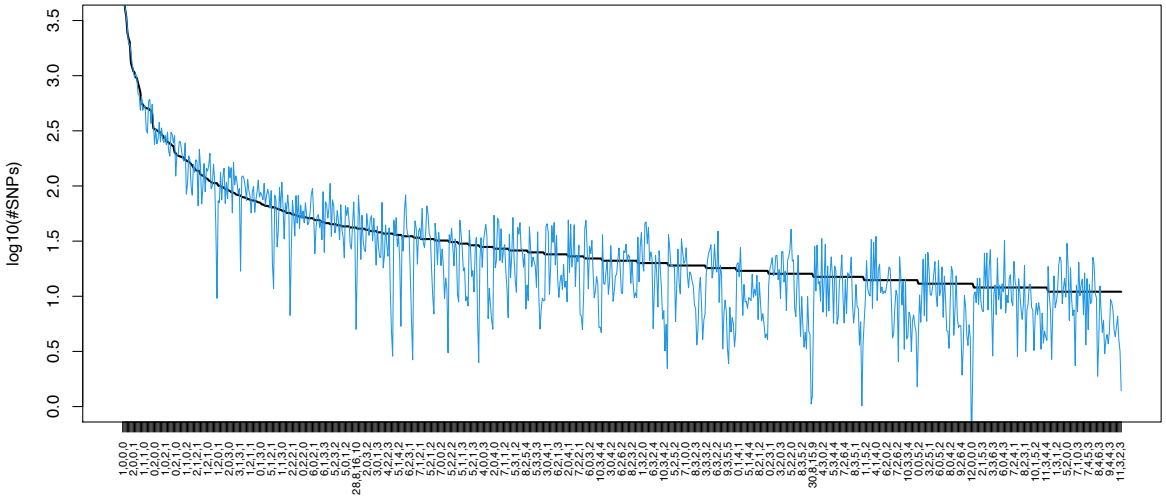

Fig. S10.
Fit of the expected to observed four-dimensional (4D)-SFS under the best model evaluated ('pscc_ful_col1') for *Pareledone turqueti*. Only entries with more than 10 SNPs are shown. Entries in the x-axis are indicated by column in the format of (AS, RS, EA, WS), and numbers within each entry correspond to the count of the derived allele in Amundsen Sea (AS), Ross Sea (RS), East Antarctica (EA) and Weddell Sea (WS). Solid black line represents observed SFS, blue line represents averaged expected SFS. Averaged expected SFS was obtained from 100 SFS approximated with 500,000 coalescent simulations under the parameters that maximised the likelihoods.

Table S1.

Demographic parameters inferred in the best model (psccc_full_col1) in *Pareledone turqueti*. Maximum-likelihood (ML) parameter estimates were extracted from the best run with the highest composite likelihood among 100 replicates. Probability of emigration (m) from pop i to pop j is denoted as MIGij looking backward in time. Number of migrants per generation from pop j to pop i is denoted as IM_MIGij$, and is scaled as 2Nm (2N = population effective sizes in diploid), looking forward in time. Effective population sizes are given in the number of haploids (N). Estimations of timing of events are given in the number of generations (gen) and years. The 95% confidence intervals (CI) were generated from 100 block-bootstrapped datasets. Abbreviations: Weddell Sea (WS), Amundsen Sea (AS), Ross Sea (RS), East Antarctica (EA).

Parameter	Parameter description	ML estimate	95% CI	
			Lower bound	Upper bound
NEA$	Effective population size of EA after T2	1456	1281	230145
NWS$	Effective population size of WS after T2	20071	25482	142309
NAS$	Effective population size of AS after T2	107251	3213	772442
NRS$	Effective population size of RS after T2	12339	14592	332691
NEAC$	Effective population size of EA after T1	570182	32935	730432
NWSC$	Effective population size of WS after T1	663252	231105	923873
NASC$	Effective population size of AS after T1	23384	12140	684397
NRSC$	Effective population size of RS after T1	301550	33424	747585
NANC2$	Effective population size of the ancestral population of AS, WS, RS and EA after T0	1332567	1428602	3501509
NANC1$	Effective population size of the ancestral population of AS, WS, RS and EA before T0	8694	9564	32259
T1 (gen)	Time of trans-West Antarctic seaway connectivity between WS-RS (in generations)	5797	5638	22090
T0 (gen)	Time of demographic change in the ancestral population of WS, AS, RS and EA (in generations)	147535	158889	500302
T2 (gen)	Time of contemporary gene flow between WS-AS-RS-EA driven by circumpolar current (in generations)	1851	2372	16305
T1 (year)	Time of trans-West Antarctic seaway connectivity between WS-RS (in years)	69564	67656	265080
T0 (year)	Time of demographic change in the ancestral population of WS, AS, RS and EA (in years)	1770420	1906668	6003624
T2 (year)	Time of contemporary gene flow between WS-AS-RS-EA driven by circumpolar current (in years)	22212	28464	195660
MIG10$	Probability of emigration from AS to WS after T2 (backward in time)	5.83E-08	1.90E-09	2.38E-03
MIG30$	Probability of emigration from EA to WS after T2 (backward in time)	1.25E-02	3.63E-05	1.33E-02

MIG01$	Probability of emigration from WS to AS after T2 (backward in time)	9.40E-04	7.77E-05	6.85E-04
MIG21$	Probability of emigration from RS to AS after T2 (backward in time)	1.54E-03	1.17E-08	1.23E-03
MIG12$	Probability of emigration from AS to RS after T2 (backward in time)	5.67E-05	7.42E-10	5.57E-03
MIG32$	Probability of emigration from EA to RS after T2 (backward in time)	8.81E-03	5.61E-08	8.78E-03
MIG03$	Probability of emigration from WS to EA after T2 (backward in time)	1.54E-04	1.83E-09	2.04E-04
MIG23$	Probability of emigration from RS to EA after T2 (backward in time)	7.83E-04	1.19E-05	6.76E-04
MIG02C$	Probability of emigration from RS to WS after T1 (backward in time)	1.05E-08	2.20E-10	3.14E-06
MIG20C$	Probability of emigration from WS to RS after T1 (backward in time)	1.13E-08	2.92E-10	4.80E-06
IM_MIG10$	Number of immigrants per generation from WS to AS after T2 (forward in time)	3.13E-03	3.05E-06	921
IM_MIG30$	Number of immigrants per generation from WS to EA after T2 (forward in time)	9	2.33E-02	1527
IM_MIG01$	Number of immigrants per generation from AS to WS after T2 (forward in time)	9	1	49
IM_MIG21$	Number of immigrants per generation from AS to RS after T2 (forward in time)	10	8.52E-05	205
IM_MIG12$	Number of immigrants per generation from RS to AS after T2 (forward in time)	3	1.19E-06	2152
IM_MIG32$	Number of immigrants per generation from RS to EA after T2 (forward in time)	6	3.60E-05	1011
IM_MIG03$	Number of immigrants per generation from EA to WS after T2 (forward in time)	2	2.33E-05	15
IM_MIG23$	Number of immigrants per generation from EA to RS after T2 (forward in time)	5	8.68E-02	113
IM_MIG02C$	Number of immigrants per generation from WS to RS after T1 (forward in time)	1.58E-03	3.67E-06	1
IM_MIG20C$	Number of immigrants per generation from RS to WS after T1 (forward in time)	3.76E-03	3.37E-05	2

485

Table S2.

Results of outgroup-*f*3-statistics between pairs of populations. As *f*3 value increases, more derived allele frequency is shared between population A and population B related to an outgroup population (population C). Abbreviations: Weddell Sea (WS), South Shetland Islands (SHE), Amundsen Sea (AS), Ross Sea (RS), East Antarctica (EA), Shag Rocks and South Georgia (SGSR; samples combined). Z-score values > 3 or < -3 = significance, stderr=standard error, nsnps=number of SNPs involved in the statistics.

population A	population B	population C	*f*3	stderr	Zscore	nsnps
AS	RS	SRSG	0.054015	0.001107	48.80	92000
RS	EA	SRSG	0.046025	0.001025	44.92	93586
RS	WS	SRSG	0.045840	0.000870	52.71	105128
RS	SHE	SRSG	0.043447	0.000787	55.24	97556
AS	EA	SRSG	0.043384	0.000957	45.35	86461
AS	SHE	SRSG	0.042471	0.000841	50.47	90359
AS	WS	SRSG	0.042254	0.000847	49.88	99122
WS	SHE	SRSG	0.039757	0.000702	56.63	102545
WS	EA	SRSG	0.039279	0.000876	44.84	99159
SHE	EA	SRSG	0.030848	0.000714	43.21	92090

Table S3.

Results of D-statistic between (in the form of BABA-ABBA) examining patterns of alleles sharing across four populations, and indicates whether there is excess allele sharing between distinct populations. Top panel: D-statistic is presented in the form of D(Pop, SHE, WS, Out), which examines whether there is excess allele sharing between SHE and WS (D<0; ABBA) or Pop and WS (D>0; BABA). Bottom panel: D-statistic is presented in the form of D(Pop, EA, WS, Out), which examines whether there is excess allele sharing between EA and WS (D<0; ABBA) or Pop and WS (D>0; BABA). Abbreviations: Weddell Sea (WS), South Shetland Islands (SHE), Amundsen Sea (AS), Ross Sea (RS), East Antarctica (EA), Shag Rocks and South Georgia (SRSG; samples combined as an outgroup population [Out]). Z-score values > 3 or < -3 = significance, stderr=standard error, nsnps=number of SNPs involved in the statistics.

D-statistic presentation	W	X	Y	Z	*D*	stderr	Zscore	BABA	ABBA	nsnps
D(Pop, SHE, WS, Out) / *D*(W, X, Y, Z)	AS	SHE	WS	SRSG	0.0113	0.001857	6.084	1576	1541	120857
	RS	SHE	WS	SRSG	0.0284	0.001838	15.447	1554	1468	120857
D(Pop, EA, WS, Out) / *D*(W, X, Y, Z)	AS	EA	WS	SRSG	0.0130	0.002007	6.465	1638	1596	120857
	RS	EA	WS	SRSG	0.0295	0.001870	15.770	1616	1523	120857

Table S4.

Summary of likelihoods for the model tested at step 1 in *Pareledone turqueti*. Model label corresponds to model label in fig. S3-S4. Delta AIC and relative likelihoods were calculated following Excoffier et al. (2013) (*34*). Abbreviations: Lhood = log likelihoods, AIC = Akaike Information Criterion.

Model label	log10(Lhood)	Number of parameters	AIC	Delta AIC	Relative likelihood (Akaike's weight of evidence)
psc_nocol	-175298.50	17	807458.91	0.00	1.00
psc_fulcol1	-175301.95	19	807478.78	19.87	0.00
psc_parcol	-175311.88	19	807524.54	65.63	0.00
psc_parcol2	-175334.40	19	807628.23	169.32	0.00
psc_conflow	-175344.44	12	807660.49	201.59	0.00
psc_fulcol2	-175583.38	23	808783.05	1324.15	0.00

Table S5.

Summary of likelihoods for the model tested at Step 2 in Pareledone turqueti. Model label corresponds to model label in fig. S3-S4. Delta AIC and relative likelihoods were calculated following Excoffier et al. (2013) (*34*). Abbreviations: Lhood = log likelihoods, AIC = Akaike Information Criterion.

Model label	log10(Lhood)	Number of parameters	AIC	Delta AIC	Relative likelihood (Akaike's weight of evidence)
psccc_fulcol1	-174981.32	23	806009.97	0.00	1.00
psccc_parcol	-174997.22	23	806083.19	73.22	0.00
psccc_parcol2	-175000.91	23	806100.20	90.24	0.00
psccc_fulcol3	-175010.87	25	806150.08	140.11	0.00
psccc_nocol	-175022.77	21	806196.88	186.91	0.00
psccc_fulcol2	-175037.78	27	806278.02	268.05	0.00
psccc_fulcol4	-175053.17	25	806344.88	334.92	0.00
psccc_conflow	-175178.67	16	806904.94	894.98	0.00

Data S1. (separate file: DataS1-S2.xlsx)

Sample information of *Pareledone turqueti* (n=96) sequenced with target capture sequencing of ddRAD loci.

Data S2. (separate file: DataS1-S2.xlsx)

Sample information of all Southern Ocean octopod samples (n=440, including 22 technical replicates) sequenced with ddRAD sequencing.